Geophysical Prospecting, 2001, **49**, 374–386

Adaptation of prestack migration to multi-offset ground-penetrating radar (GPR) data

Donatienne Leparoux,[1] Dominique Gibert[2] and Philippe Côte[3]

[1]*Bureau de Recherche Géologique et Minière, BP 6009, 45060 Orléans,* [2]*Géosciences Rennes, Université Rennes 1, campus Beaulieu, 263 av Général Leclerc, 35700 Rennes, and* [3]*Laboratoire Central des Ponts et Chaussées, BP 4129, 44341 Bouguenais Cedex, France*

Received March 2000, revision accepted November 2000

ABSTRACT

In adapting the prestack migration technique used in seismic imaging to the inversion of ground-penetrating radar (GPR) from time- to depth-sections, we show that the theoretical integral formulation of the inversion can be applied to electromagnetic problems, albeit with three assumptions. The first two assumptions concern the electromagnetic characteristics of the medium, primarily that the medium must be perfectly resistive and non-dispersive, and the third concerns the antennae radiation pattern, which is taken to be 2D. The application of this adaptation of the inversion method is confirmed by migrating actual GPR measurements acquired on the test site of the Laboratoire Central des Ponts et Chaussées. The results show good agreement with the geometry of the structures in the medium and confirm that the possible departure from the assumption of a purely resistive medium has no visible effect on the information concerning the geometry of scattering and reflecting structures. The field experiments also show that prestack migration processing is sufficiently robust with regard to the assumption of a non-dispersive medium. The assumption of a 2D antennae radiation pattern, however, produces artefacts that could be significant for laterally heterogeneous media. Nevertheless, where the medium is not highly laterally heterogeneous, the migration gives a clear image of the scattering potential due to the geometry of structural contrasts in the medium; the scatterers are well focused from diffraction hyperbolae and well localized. Spatial geometry has limited dimensional accuracy and positions are located with a maximum error equal to the minimum wavelength of the signal bandpass. Objects smaller than one wavelength can nevertheless be detected and well focused if their dielectric contrasts are sufficiently high, as in the case of iron or water in gneiss gravels. Furthermore, the suitability of multi-offset protocols to estimate the electromagnetic propagating velocity and to decrease the non-coherent noise level of measurements is confirmed. Our velocity estimation is based on the semblance calculation of multi-offset migrated images, and we confirmed the relevance of this quantification method using numerical data. The signal-to-noise ratio is improved by summing multi-offset results after the addition of random noise on measurements. Thus the adaptation of prestack migration to multi-offset radar measurements significantly improves the resolution of the scattering potential of the medium. Limitations associated with the methods used here suggest that 3D algorithms should be applied to strongly laterally heterogeneous media and further studies concerning the waveform inversion are necessary to obtain information about the electric nature of the medium.

INTRODUCTION

To present ground-penetrating radar (GPR) time-sections in purely spatial terms, rather than as a mix of time and distance measurements, requires some inversion processing. Because of the close analogy between radar time-sections and seismic-reflection profiles, the adaptation of seismic imagery methods, such as migration to GPR imaging, can be considered. With standard GPR procedures that allow the transmitter and receiver to be at the same position (zero-offset), zero-offset seismic migration techniques can be applied to radar measurements without the need for dynamic corrections (Bitri and Grandjean 1998). In this case, some authors suggest specific techniques to evaluate the migration velocity based on iterative processes and focusing criteria (Patterson, Tealby and Allinson 1995; Jaya *et al*. 1999) or on additional tests such as field tomographic imaging or laboratory measurements of the dielectric permittivity from drill cores (Fisher *et al*. 1992b). However, these last authors conclude by advocating a test multi-offset process. In reality, it is necessary to consider the relevance of commonly used seismic multi-offset configurations, such as post- or prestack migration, for multi-offset measurements. The latter are used to provide information about the mean velocities required for the inversion of arrival times in depth-section processing.

When using post-stack migration, mean velocities are determined by the common-midpoint method whereby a normal-moveout (NMO), which is a dynamic correction, is applied to the arrival times to remove the effect of variable offsets. Several studies have successfully adapted this type of velocity analysis and dynamic correction to radar data for stratified media (Fisher, McMechan and Annan 1992a; Liner and Liner 1995; Young, Deng and Sun 1995; Greaves *et al*. 1996; Hollender, Tillard and Corin 1999). This technique is not, however, appropriate for complex media where significant diffraction events have to be considered for the radar time-section inversion; for instance, soil a few metres deep is very rarely homogeneous at the wavelengths used by radar (around 20 cm for a 500 MHz electromagnetic wave in soil).

With prestack migration, the velocity contrasts of the medium are determined from the arrival times along several common-offset profiles by taking the single-diffraction principle into account. In this way, the integral method of migration can be adopted and would be appropriate for shallow GPR studies where significant diffraction can be expected. Moreover, the prestack migration on multi-offset data needs neither other process such as NMO and DMO, nor additional measurements to evaluate the migration velocity, and thus it should provide better results in complex media. Some authors have proposed near-offset methods by introducing the eccentricity parameter (Stolte, Ristow and Nick 1994) or by optimizing the time calculation (Botelho, Mufti and Neto 1998). We propose testing the prestack migration for multi-offset GPR measurements on a simple case. Our objectives are to study the theoretical applicability of the migration principle to GPR data and to analyse its robustness, as well as the quality of the resulting migrated image, at an *a priori* known site. This work is a first step before further tests on complex media, where the comparison with other methods could be interesting.

In the following discussion, we demonstrate that the direct problem is adaptable to GPR measurements under certain assumptions. This implies that the inverse problem (i.e. migration) is also adaptable. We explain the principles of this migration in the depth domain using the generalized Radon transform (Miller, Oristaglio and Beylkin 1987) and follow this with the derivation of a quantitative method of estimating the migration velocity using the semblance of migrated scans at various offsets. Finally, we apply prestack migration to radar measurements obtained at the Laboratoire Central des Ponts et Chaussées (LCPC) test site (Chazelas 1996) to test the validity of the technique. The improvement in the signal-to-noise ratio due to the multi-offset process is also checked, and we show that it confirms the relevance of multi-offset measurements in GPR.

THE MIGRATION PRINCIPLE

The migration of seismic waves was first carried out using a geometric technique with curve charts. In this approach, migration was considered as a reconstruction method of earth reflectors from surfaces of equal reflection times, which were shown to be the surfaces of maximum concavity (Hagedoorn 1954). The use of the scalar wave propagation equation for the migration theory appeared some 15 years later with the concept of extrapolating the field to give imaging depths. In this, the image of the reflectors is built up from a combination of the down- and up-going fields, the reflectors lying where the phase surfaces of the two fields coincide (Claerbout 1970, 1971, 1972), and the computation is carried out in the frequency domain, assuming a large spectral band in order to remove the ambiguity of coincident phase positions. Arising out of this concept came migration in the f–k domain (Gazdag 1978; Stolt 1978), and at about the same time, integral migration methods were further

developed (Schneider 1978). 'Diffraction-stack' migration proved to be appropriate as a mathematical inversion technique for calculating the medium scattering potential from seismic measurements and it was further refined by Bleistein (1987) and Miller *et al.* (1987). Here, based on the high-frequency assumption and on the Eikonal equation, the time information is transformed directly into a depth image. We propose that if it is possible to describe electromagnetic wave propagation with the scalar wave propagation equation, it should be possible to adapt the seismic migration concept to radar data, since both the direct and inverse problems are based on this equation.

The Helmholtz equation for electromagnetic waves

For radar measurements recorded in TE mode in a perfectly resistive 2D medium (x_1, x_3), the electric field variation can be described by the equation,

$$\varepsilon \frac{\partial^2}{\partial t^2} E_{x_2} = \frac{\partial}{\partial x_3}\left(\frac{1}{\mu}\frac{\partial}{\partial x_3} E_{x_2}\right) + \frac{\partial}{\partial x_1}\left(\frac{1}{\mu}\frac{\partial}{\partial x_1} E_{x_2}\right), \quad (1)$$

where the wavefield is propagating in the plane (Ox_1,Ox_3), and where (Ox_2) is the transverse direction. $E_{x_2}(x_1, x_3, t)$ is the transverse electric field component, ε is the dielectric permittivity of the medium (considered here as a real number) and μ is the magnetic permeability of the medium.

As the magnetic permeability of geological materials currently probed by GPR can be considered to be the same as in a vacuum, i.e. $\mu = \mu_0 = 4\pi\ 10^{-7}$ H/m, (1) can be written as

$$\varepsilon\mu_0 \frac{\partial^2}{\partial t^2} E_{x_2} - \nabla^2 E_{x_2} = 0. \quad (2)$$

This is the scalar wave propagation equation and it is mathematically similar to the acoustic wave equation. In the frequency domain, it is similar to the Helmholtz equation,

$$\varepsilon\mu_0\omega^2 \overline{E}_{x_2} - \nabla^2 \overline{E}_{x_2} = 0, \quad (3)$$

where ω is the angular frequency, i.e. the dual variable of time t, of the propagating wave and $\overline{E}_{x_2}(x_1, x_3, \omega)$ is the Fourier transform of $E_{x_2}(x_1, x_3, t)$.

As the direct problem is described by the Helmholtz equation, we can, by analogy to acoustic propagation, consider the inverse problem as migration. However, adaptation of acoustic migration to the electromagnetic case involves a set of assumptions. The first assumption arises from the approximation of the problem as 2D, whereas the antennae pattern is 3D: the distortion of the migration, which arises from the 2D approach, must be taken into account when results are analysed. A second assumption concerns the resistivity of the medium, which is taken to be infinite, whereas in reality, natural media are often conductors. In the same way, we assume the dielectric permittivity to be a real, non-frequency-dependent number. The resistivity and permittivity conditions can be combined by assuming that the effective dielectric permittivity is real and non-frequency dependent. In fact, dispersion phenomena due to frequency dependence result in distortion of the wave shape, while the imaginary part of the effective permittivity essentially explains the attenuation effects on the propagating wave (Bano 1996). Consequently, information contained in the signal amplitudes concerning attenuation and wavelet distortion will be ignored because of the assumptions about the effective permittivity. However, the proposed migration inverts the arrival times of radar pulses, without considering any effects on amplitude other than attenuation due to the geometrical spreading of the waves. So far, we can consider that it describes the geometrical structures of the reflectors in the medium without providing information about the nature of the propagating medium. However, distortions of signal due to attenuation and dispersion can affect the processed image. Thus the next step is to test the effect of the three assumptions described by validating the migrated depth-sections with real data.

We have shown from a purely theoretical point of view that under the three assumptions the electromagnetic wave propagation can be described by (3), which is the Helmholtz equation in a non-dispersive and non-attenuating medium. The solution of the direct problem therefore requires the solution of the Helmholtz equation in a medium with contrasting propagation velocities, and the inverse problem, namely migration, necessitates finding these velocity contrasts (which we refer to as scattering potentials) from the solution of the Helmholtz equation.

Direct problem: single scattering model

In order to explain the migration principle, we consider the more general 3D spatial case with the following notation. A parameter $x = (x_1, x_2, x_3)$ is introduced to describe the spatial coordinates. The receiver position r, the source position s and any point position m are given as follows: $r = r(x)$, $s = s(x)$, $m = m(x)$. For this approach, the source is considered as an impulsive delta function of space and time, $\delta(x, t)$, and the solution of the propagation equation is the Green's function of the medium. Taking $v = 1/\sqrt{\varepsilon\mu_0}$ as the propagation velocity in the medium and including

variations $f(x)$ superimposed on a velocity v_0, we obtain

$$\frac{1}{v^2(x)} = \frac{1}{v_0^2(x)} + f(x). \tag{4}$$

The perturbation $f(x)$ is termed the scattering potential.

The solution of the propagation equation in such a medium, i.e. the total field at a point in the medium (e.g. at the receiver r), is the sum of the primary field and the diffracted field at this receiver r. The primary field emitted by the source s, i.e. $E_p(r, s, \omega)$, is the propagating field in a homogeneous medium with a velocity v_0. In the case of a perfectly impulsive source, it is the Green's function, $G_0(r, s, \omega)$, of this homogeneous medium for the variables (r, s, ω). The diffracted field at the receiver r is given by

$$E_d(r, s, \omega) = \omega^2 \int d^3x \; G_0(r, m, \omega) \; f(x) \; E(m, s, \omega), \tag{5}$$

where $G_0(r, m, \omega)$ is the defined Green's function for the angular frequency ω from the scatterer located at m to the receiver r, and $E(m, s, \omega)$ is the total electric field emitted from the source s and received at m.

The radar response records variations in the diffracted field in the probed medium. These depend on the total field, i.e. on the primary field and on the diffracted field from each scatterer for all the volume illuminated by the source. In order to remove this dependence on the diffracted part of the total field and to linearize the equation, the total field is considered as equivalent to the primary field, and then the first Born approximation, which is the approximation of single scattering, is carried out. This means that each point of the medium is considered to be illuminated only once and multiple scattering is ignored by assuming small velocity contrasts $f(x)$ in the medium. The diffracted field is then given by

$$E_d(r, s, \omega) = \omega^2 \int d^3x \; G_0(r, m, \omega) \; G_0(m, s, \omega) \; f(x). \tag{6}$$

Green's function formulation

The Green's function is formulated according to the first-order asymptotic approximation, which is a high-frequency approximation. Thus we have

$$G_0(m, n, \omega) = A(m, n) e^{i\omega\tau(m,n)}, \tag{7}$$

where $\tau(m, n)$ is the traveltime function between the two points n and m which satisfies the Eikonal equation,

$$[\nabla_x \tau(m, n)]^2 = \frac{1}{v_0^2}, \tag{8}$$

and $A(m, n)$ is the Green's function amplitude, which satisfies the transport equation between the two points n and m.

By substituting this Green's function formulation into (6) and transforming it to the time domain, the diffracted field becomes

$$E_d(r, s, t) = -\frac{\partial^2}{\partial t^2} \int d^3x \; A(r, m, s) \; \delta[t - \tau(r, m, s)] \; f(x). \tag{9}$$

It can be seen that the diffracted field E_d, which constitutes the radar images, is the integration (twice differentiated with respect to time) of the scattering potential in the medium for all points where the traveltime τ is equal to the arrival time t, weighted by the Green's function amplitude. Note that a point from the radar image is linked to a set of points in the medium by the traveltime function and in this way by the Eikonal equation.

The direct problem is therefore solved. To solve the inverse problem (6) is shown to be the formulation of a Radon transform and can be inverted in the same way.

Inverse problem: inversion of the generalized Radon transform

The analogy between the diffracted field form of (9) and the formulation of the Radon transform twice differentiated has been shown by Miller *et al.* (1987), and hence it is known as the 'generalized Radon transform'. This analogy enables us to invert the scattering potential $f(x)$. In the 2D spatial case, it is written as

$$f(x) = \frac{1}{\pi^2} \int d^2D(r, m, s) \frac{|\cos^3\alpha(r, m, s)|}{v_0^3(x) A(r, m, s)} E_{x_2,d}(r, s, t = \tau_0), \tag{10}$$

which is the migration formulation. Here, the location of $m(x)$ defines the time t by the traveltime value $\tau(s, m, r)$. The integration is carried out at the intersection point of the isochrones (i.e. the space surfaces for which the traveltime function is constant). The set of planes constituting the integration area corresponds to the set of isochrones. These surfaces are not plane but, in view of the asymptotic approximation constituting the ray theory, it is possible to regard them locally as equivalent to their tangents D at the integration point x by introducing a weighting term

$$\frac{\cos^2\alpha(r, m, s)}{v_0^2(x)},$$

where $\alpha(r, m, s)$ is the angle between the incident ray and the diffracted ray at m (Miller *et al.* 1987).

As a radar image point $E_{x_2,d}(r, s, t)$ is linked to a set of

space-points describing an isochrone, the value $f(x)$ at the space-point x is linked to a set of points on the radar image for which $t = \tau_0$. The connection between the two domains (i.e. space and radar image) is obtained by the Eikonal equation. Finally, the inversion (known as migration) is carried out by integration at the intersection points of the isochrones for each pair of transmitter and receiver locations, s and r, respectively.

Numerical calculation

In the 2D discrete domain of data, the integration on the isochrones becomes a summation. With the numerical method used (Noble *et al*. 1996), each measurement point on the isochrone is put into the corresponding isochrones of the traveltime charts, calculated by the Eikonal equation for each position of the transmitter–receiver pair. The resulting charts for different transmitter–receiver geometries are superimposed and the values of the measurements at the intersection points of the isochrones are then added (Fig. 1). The traveltimes are calculated by finite differences (Podvin and Lecomte 1991) from the velocity assumption and the Eikonal equation. The grids are staggered. Arrival times are calculated for all the propagation modes at each point of the grid and, according to the Fermat principle, only the first one is kept.

DETERMINING THE MIGRATION VELOCITY

In order to migrate data by the method described above, the propagating velocity in the medium must be known. It can be evaluated from multi-offset measurements. Initially a migrated image for each offset is obtained using the calculation indicated in Fig. 1, which symbolizes the migration principle for a constant-offset radar image. If the velocity used in this calculation is correct, then the migrated images from several offsets will be identical. By quantifying the similarity between several common-offset migrated images, it is then possible to evaluate the correct migration velocity.

In the seismic reflection technique, the migration velocity is usually found by analysing the coherence panels (Adler 1996) that are calculated from migrated profiles of several offsets at the same distance from the origin of the profile. If the migrated velocity is correct, the migrated profiles are identical and horizontal lines will appear in the plane perpendicular to the common-offset images. The coherence, calculated in this plane, is a maximum for the correct velocity. Figure 2(a) shows synthetic radar data obtained by the finite-difference method (Leparoux 1997), where the background medium velocity is equal to 0.15 m/ns. The migrated image obtained with this velocity (Fig. 2b) shows a scatterer focused at 1.7 m depth. This is the top of a rock inclusionEQ the bottom of which is indicated by the second scatterer on the migrated image, at 2.2 m depth. A horizontal surface is also imaged at 3.1 m depth and a folded surface at 4 m depth. Figure 3 shows panels obtained with three different velocities: 0.11 m/ns, 0.15 m/ns, 0.18 m/ns. The offset increases from 0.75 m to 2.7 m with a step of 0.3 m. For the correct velocity on the middle image, the individual structural elements produce horizontal lines. This does not occur on the other two panels. Instead of the coherence, the semblance calculation, which is a quantified method commonly used in velocity analyses (Cohen and Stockwell 1997), is used here for each of the panels to evaluate the similarity between common-offset migrated images. It measures the statistical distance between values of several migrated offsets for a given location on the profile at a given depth. The semblance is given by

$$S(z) = \frac{\left[\sum_{j=0}^{n-1} a(z,j)\right]^2}{n \sum_{j=0}^{n-1} [a(z,j)]^2}, \tag{11}$$

where $S(z)$ is the semblance at the depth z, $a(z, j)$ is the amplitude of the migrated signal at depth z using data measured with offset j, and n denotes the number of non-zero values summed.

The semblance of the synthetic migrated profile versus the migration velocity (Fig. 4) shows a peak for the correct velocity. The maximum contour, shown in Fig. 4(b), corresponds to an extended zone because of signal oscillations; the maximum relative error is 10% (0.165 m/ns instead of 0.15 m/ns). This test on theoretical data shows that it is possible to use the semblance calculation to determine the velocity migration from multi-offset data.

MIGRATION ON THE TEST SITE: VALIDATION OF THE TECHNIQUE

Test site

A test site was built by the LCPC to study the possibilities of using geophysical methods to investigate subsurface properties for civil engineering works, without the need for trenches

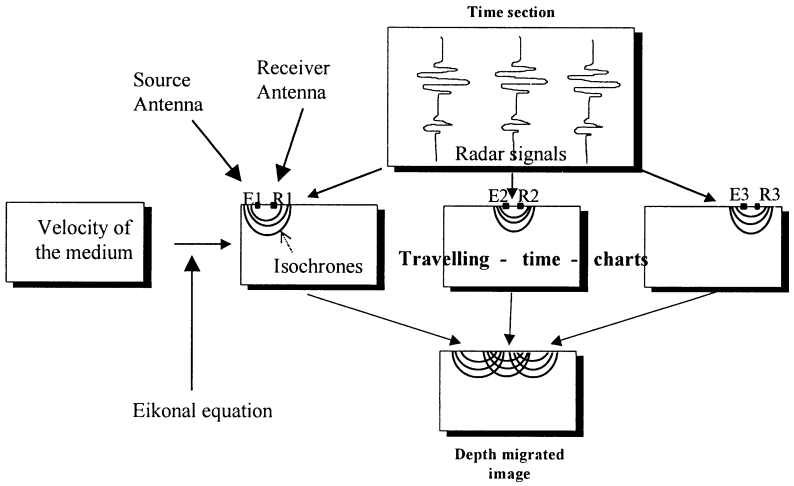

Figure 1 Diagram of the migration principle for a common-offset time-section acquired in a medium with constant velocity.

(Chazelas 1996). This site is ideal for testing radar imagery methods because it contains 1D, 2D and 3D objects that are the same size as structures found in civil engineering, such as rock inclusions, pipes and walls. Because the positions of these objects and the nature of the surrounding medium are well known, it is possible to compare different measurement protocols and processing techniques (Grandjean, Gourry and Bitri 2000). The part of the site selected for our GPR test contained not only 2D heterogeneities, in agreement with the 2D assumption, but also 3D structures to test the impact of the 2D assumption in this case. Knowing the depth of the surrounding medium and the size of the objects, we used 500 MHz antennae for the radar measurements.

The boundaries and bottom are sloped to facilitate rainwater run-off. The test site consists of five cross-trenches from 19 m to 24.6 m long, filled with media of specific nature (Fig. 5a), and the depth of the trenches varies along the site length (perpendicular to the trench length) between 3.3 m and 4.7 m to give a 5% slope.

The fourth trench, which was used for our study (Fig. 5b),

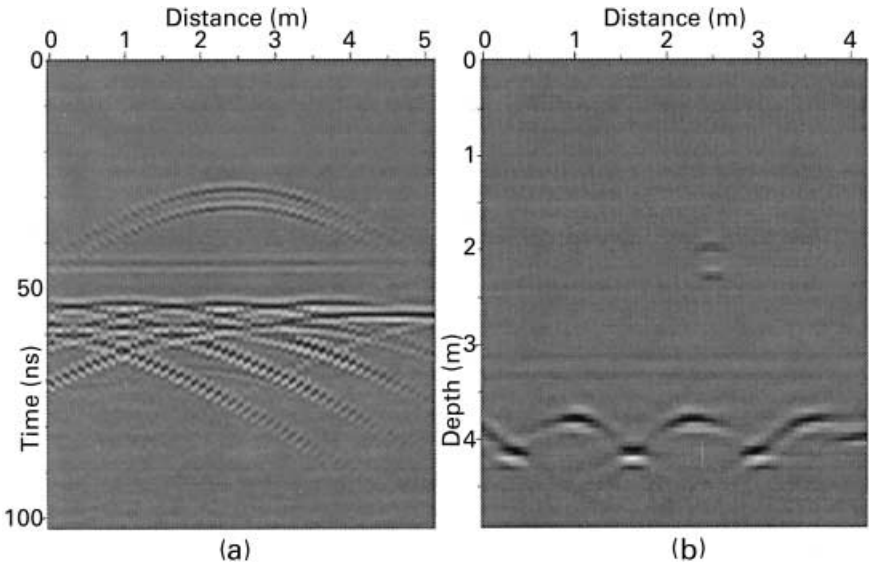

Figure 2 Prestack migration of a synthetic time-section. (a) Common-offset synthetic time-section. (b) Stacked migrated image from the different synthetic common-offset data (the offset ranges between 0 and 2.7 m).

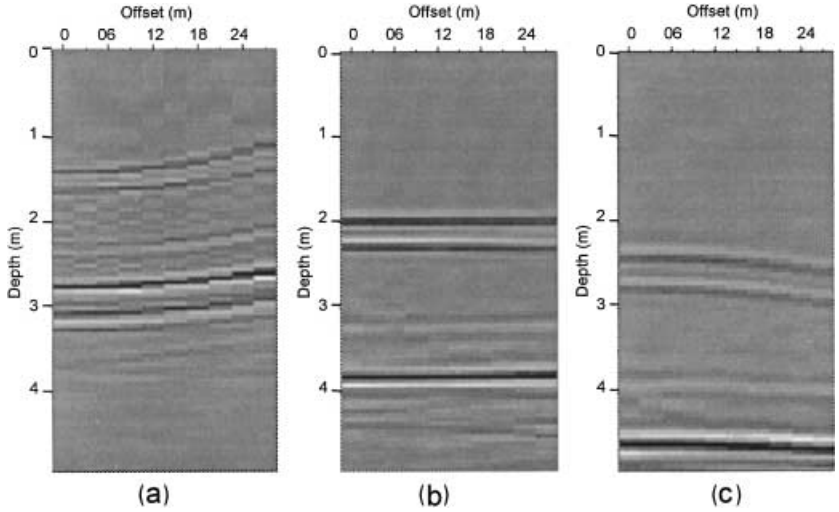

Figure 3 Panels showing common-offset migrated data obtained from numerical data similar to Fig. 2 data: (a) for a migration velocity of 0.11 m/ns; (b) for a migration velocity of 0.15 m/ns; (c) for a migration velocity of 0.18 m/ns.

contained three sets of three pipes and a large concrete nozzle (diameter 0.5 m) buried in gneiss gravels with a grain size limited to between 14 and 20 mm. The first pipe in each set of the three was an empty iron pipe (diameter 0.08 m), the second was a water-filled PVC pipe (diameter 0.1 m) and the third was an empty PVC pipe (0.1 m Ø). The distance between the pipes varied with each set: 1.0 m for the lower set at a depth of 2.1 m, 0.7 m for the middle set at a depth of 1.5 m, and 0.5 m for the upper set at a depth of 0.9 m. The large concrete nozzle buried in this part of the test site could be considered to be a 3D object because of its joints. The site depth in this area was 4.10 m.

Measurements

Measurements were carried out at 500 MHz with seven offsets between 0.75 m and 1.55 m. The sampling intervals were 0.02 m in space and 0.2 ns in time. Figure 6 shows measurements recorded with an offset of 0.75 m between the

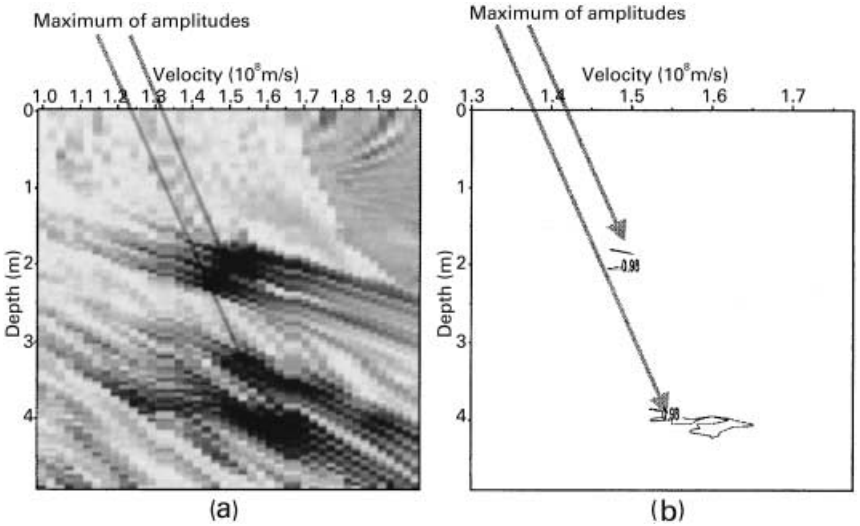

Figure 4 Semblance panel obtained from the several common-offset migrated data obtained using numerical data similar to Fig. 2 data: (a) contrasts image of semblance; (b) contours of semblance equal to 0.98.

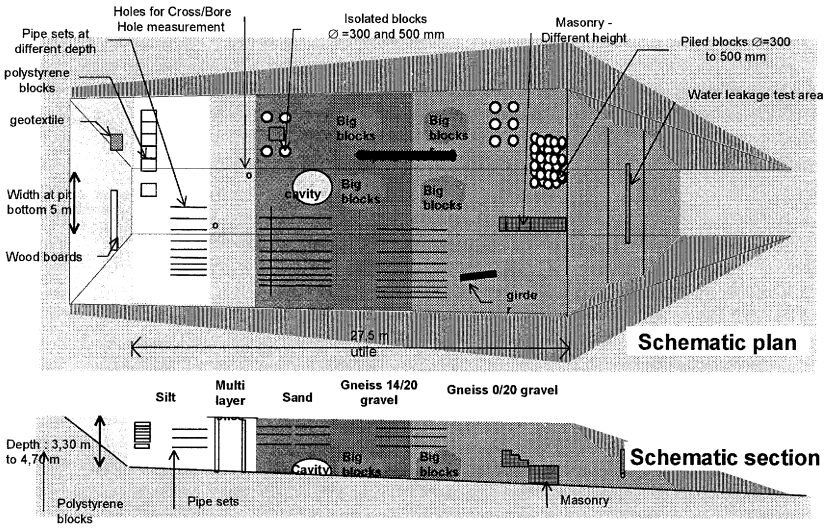

(a)

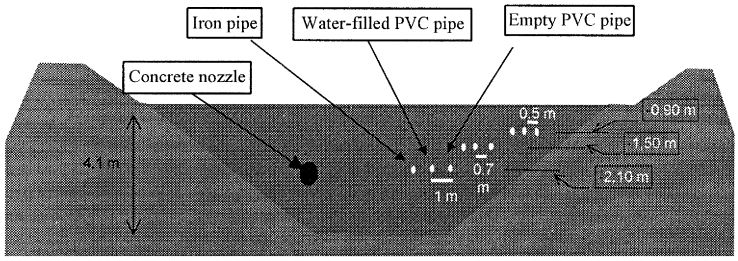

(b)

Figure 5 (a) Schematic plan and schematic section of the LCPC test site (Chazelas 1996). (b) Cross-section of the part of the test site used for migration validation.

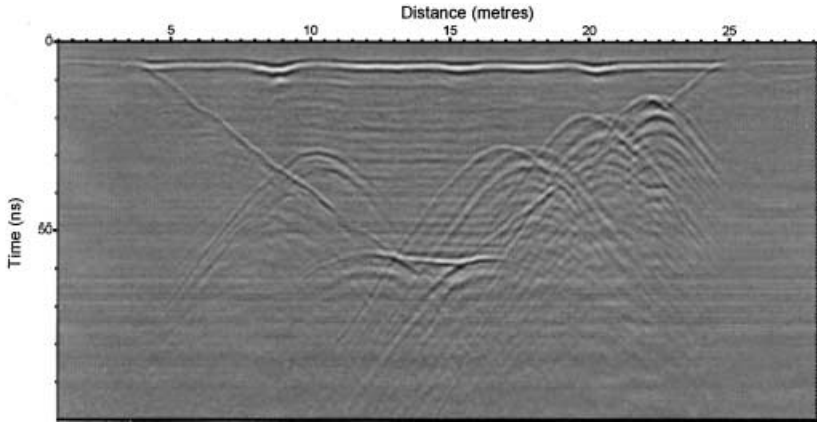

Figure 6 GPR measurements on the test site using two 500 MHz antennae and an offset of 0.75 m.

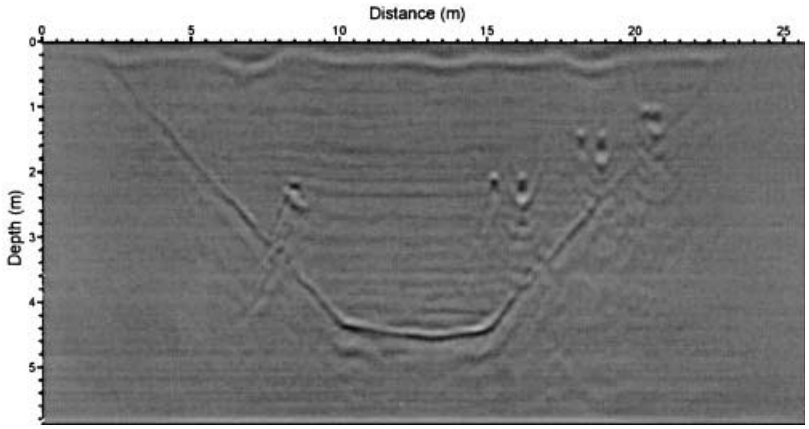

Figure 7 Stacked migrated test site measurements acquired with several offsets (0.75 m, 0.85 m, 0.95 m, 1.15 m, 1.25 m, 1.35 m, 1.55 m) and a migration velocity of 0.159 m/ns.

two antennae. Sloped continuous echoes corresponding to the lateral boundaries of the site can be clearly seen. The horizontal echo at 60 ns corresponds to the bottom of the site. The corners between the lateral boundaries and the site bottom are seen to generate diffraction hyperbolae. The other hyperbolae on the image are due to the pipes, and it can be seen that some interfere with one another. On the left of the image, a second hyperbola geometry can be seen beneath the hyperbola due to the concrete nozzle. This could be due to the bottom of the nozzle or it could be a lateral echo coming from the nozzle joints. On the right of the image, despite the interference patterns, two series of hyperbolae due to the pipes can be seen at each depth. In each case, the empty PVC pipe does not appear to have given a sufficient echo to be detected. Conversely, the PVC pipe full of water (in the middle of each set) gives multiple echoes that form a series of superimposed hyperbolae. The iron pipes do not generate the same radar response: no ringing effect is observed.

The first quasi-horizontal echo at the top of the image corresponds to the direct wave at the soil surface propagating between the two antennae. The modification of its arrival time could be due to an infiltration of water giving surficial zones with a lower propagating electromagnetic velocity than the dry medium. The continuous and periodic reflections forming horizontal echoes may be generated by the compaction of different layers of gneiss gravel during the filling of the trench. However, these echoes are very weak and the site can be considered as a homogeneous medium containing different perfectly localized scatters.

Table 1 Geometry of the test site and the objects it contains: comparison between imagery results and real dimensions

	Depth			Diameter			Laps		
Object	Real (m)	Imaged (m)	Error (%)	Real (m)	Imaged (m)	Error (%)	Real (m)	Image (m)	Error (%)
Site bottom	4.1	4.2	2.44						
Concrete nozzle	2.1	2.1	0	0.5	0.4	20			
Upper pipe set				0.08	0.2	150			
	0.9	0.9	0	0.1	0.2	100	0.5	0.4	20
				0.1					
Middle pipe set				0.08	0.2	150			
	1.5	1.3	13.33	0.1	0.2	100	0.7	0.8	14.29
				0.1					
Lower pipe set				0.08	0.2	150			
	2.1	1.9	9.52	0.1	0.2	100	1.0	1.0	0

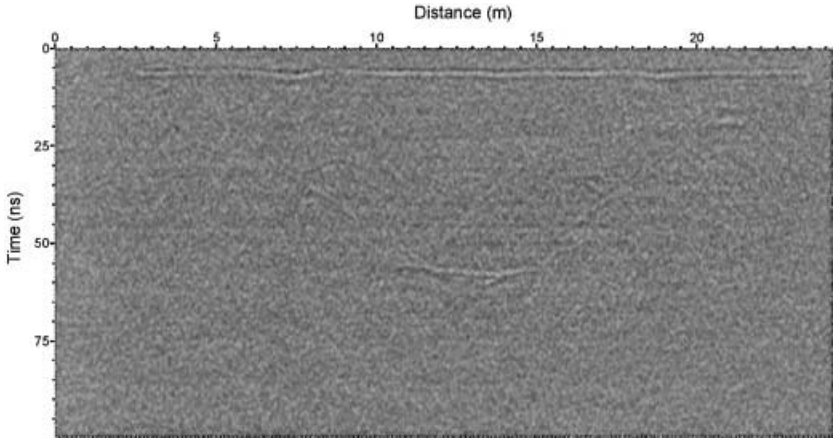

Figure 8 Random noise added to the GPR time-section acquired on the test site with two 500 MHz antennae and an offset of 0.75 m. The statistical distribution of the noise is Gaussian and was filtered between 20 MHz and 750 MHz.

Migration

The stack of the several common-offset migrated measurements acquired with the 500 MHz antennae is shown in Fig. 7. The vertical and horizontal sampling intervals are both equal to 0.02 m and the migration velocity is 0.159 m/ns (Leparoux 1997). It is seen that the site geometry is well imaged, including the lateral sloped boundaries. The three sets of pipes and the concrete nozzle are correctly located with the pipe sets on the right of the image; the empty pipe is not visible, whereas the PVC pipe full of water and the iron pipe are clearly depicted. The empty PVC pipe is not visible due to insufficient contrast with the surrounding medium, which also contains a lot of open pore spaces within the gravel.

Even if global geometry seems coincident with the site, we have to study the accuracy of the imaged medium to confirm whether or not that the assumption of a purely resistive medium affects the migrated results. In fact, dispersion phenomena generate distortion of the pulse during the propagation, which should produce different wave-shapes for the several common-offset measurements because of the different travel distances. These distortions can make different offsets non-coincident and alter the semblance calculation. The velocity estimation on this site has also been carried out by tomographic techniques (Grandjean *et al.* 2000), giving a value of 0.17 m/ns. Our error with regard to this result is lower than 7%, i.e. less than the error obtained with the numerical and non-dispersive data in the previous section. We can conclude that our velocity estimation is robust compared with tomographic techniques. The quantitative aspects, such as depth and object diameters in the migrated image, are summarized and compared with the real

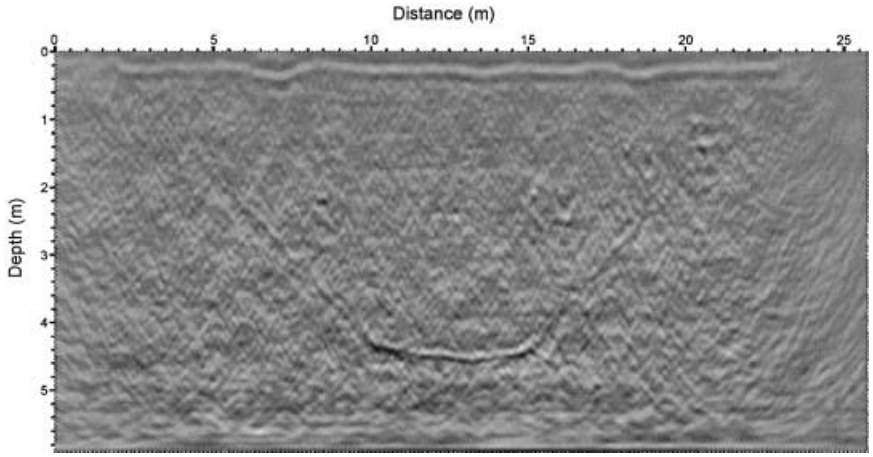

Figure 9 Migrated image of the noisy common-offset measurement shown in Fig. 8 with a migration velocity of 0.159 m/ns.

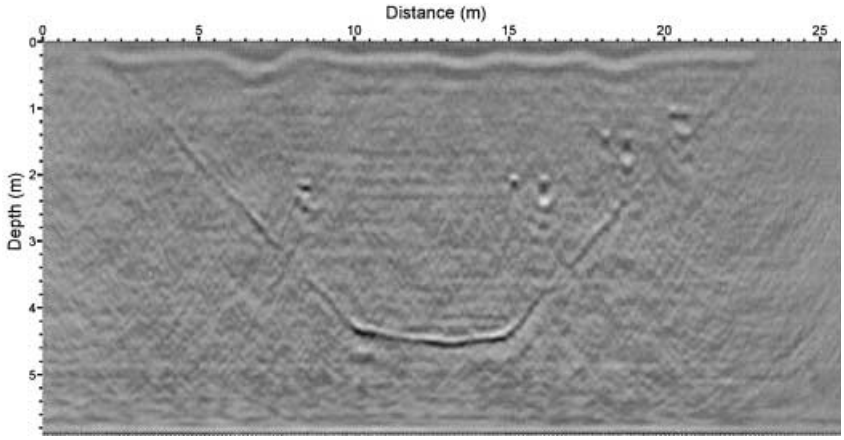

Figure 10 Stack of migrated noisy common-offset measurements for several offsets (0.75 m, 0.85 m, 0.95 m, 1.15 m, 1.25 m, 1.35 m, 1.55 m) and a migration velocity of 0.159 m/ns.

geometry of the site in Table 1. The relative errors can be as much as 150%, but the absolute corresponding errors are always less than or equal to the minimum wavelength of the signal bandpass used here (i.e. 0.2 m), which can be considered as a physical limit of the GPR probing accuracy. Even though the sizes of small objects (i.e. smaller than the minimum wavelength used) are not well determined, these objects are nevertheless detected and well focused if the dielectric contrast is sufficiently strong, as was the case for iron and water in the gneiss gravels. The good accuracy of the results, limited only by the minimum wavelength, means that this migration method can be regarded as sufficiently robust in spite of the assumption of a non-dispersive medium.

Figure 7 also shows that the ringing effect in the water-filled PVC pipe remains during the migration processing and appears as a succession of superimposed scatterers. The only way to remove this would be to apply a deconvolution before migration. However, the dispersion of electromagnetic propagating waves in geological media and the no-minimum-phase nature of the pulse make the application of the current tools of deconvolution inefficient (Turner 1994).

The effects of the assumption of a 2D radiation pattern of the antennae can be seen on the concrete nozzle. This object is well focused at a scattering point, but the migrated image is not so apparent below. The effect of a lateral structural nozzle element, such as jointing, is clearly confirmed. The migration processing calculates the scattering potential for 2D data and cannot correctly image lateral structural elements. In the case of a laterally heterogeneous medium, therefore, this assumption is not completely valid. Nevertheless, it is still possible to adapt this method to 3D phenomena.

Globally, the migration process creates an accurate image of scattering potential in the medium and it reconstitutes the field structures that have high velocity contrast with the surrounding medium. Accuracy is controlled by the wavelength of the electromagnetic pulse.

SIGNAL-TO-NOISE RATIO IMPROVEMENT

So far our interest in multi-offset measurements has been restricted to determining the migration velocity. However, it is also expected that the summation of common-offset migrated images should improve the signal-to-noise ratio. The radar images produced by the test site are not noisy (Fig. 6) and thus it is difficult to estimate the decrease in noise due to the multi-offset process. We plan to do this in further tests on measurements in complex sites. Nevertheless, in this first study, we can estimate this improvement by adding random noise to the common-offset measurements, giving it a statistical distribution equal to a Gaussian function filtered in the same pass band as the measurements (i.e. between 20 MHz and 750 MHz). Figure 8 shows the measurements acquired with an offset of 0.75 m; the signal-to-noise ratio was equal to 2 and it is no longer possible to distinguish the several echoes. Figure 9 shows the common offset of the 0.75 m image after migration where the several scattering points were not strong enough to be determined.

Random noise with the same statistical characteristics and the same amplitude level was then added to other common-offset measurements. The summation of all the migrated noisy common-offset images can be seen in Fig. 10, which shows that random noise has been reduced and the signal-to-noise ratio has been improved by this summation. The contrasts and resolutions of the added migrated noisy images

are close to the noiseless image shown in Fig. 7. The set of scatterers is well focused and the amplitude level is greater than the resulting noise amplitude, which allows clear detection without confusion. The relevance of this summation and that of the multi-offset acquisition protocol are clearly illustrated by these results.

Furthermore, when random noise is avoided by summation of several offsets, the amplitudes due to scatterers are enhanced. This confirms that all the focused scatterers remain coincident over all common-offset migrated images, even in the possible presence of dispersion phenomena.

CONCLUSION

Prestack migration by the integral method is a valuable tool for radar data and provides a realistic image of scattering contrasts of the probed medium. The electromagnetic propagation formulated by the Helmholtz equation has provided a theoretical basis for adapting the seismic migration method to ground-penetrating radar data. Since one of the *a priori* advantages of prestack migration lies in the use of multi-offset measurements to evaluate the velocities of the media, a quantification method of semblance calculation at several offsets has been developed and validated using numerical data.

The migration of real data recorded at the LCPC test site made it possible to assess the suitability of this method of prestack migration for GPR data. The results have given a realistic image of scattering potential in the medium. The site geometry is correctly reconstructed and the locations of 2D objects are correctly positioned. The image obtained focuses first arrivals from the diffraction hyperbolae, where multiple interference made the analysis of unprocessed measurements difficult. Results show that the accuracy of the technique is limited by the wavelength. For this reason, the relative error in the estimation of sizes of objects smaller than the wavelength can be large, but these objects are nevertheless detected, focused and localized if their dielectric contrast is sufficiently strong. The decrease in inconsistent echoes obtained by the summation of data from several offsets was confirmed by adding numerical noise to the measurements before migration and summation.

This application to real measurements has also enabled an assessment of the assumptions used in this study. The possible deviation from the approximation of a purely resistive medium had no major effect; the geometry of the medium was determined without knowledge of the nature of the medium. In contrast, 3D artefacts appear and could be problematic for the interpretation of the migrated image in the instance of a strongly laterally heterogeneous medium; in such cases, it would be necessary to acquire data with 3D protocols of measurements and to process them by a 3D migration algorithm.

Overall, the study has validated prestack migration by the integral method for GPR surveys. It has illustrated the capability of imaging objects smaller than the wavelength used, and it has confirmed the relevance of the multi-offset protocol to evaluate velocity and to decrease incoherent noise. We consider that the validation exercise undertaken here in a well-known homogeneous medium is sufficient justification for the future application of prestack migration to unknown media and to variable velocity media.

ACKNOWLEDGEMENTS

We thank M.S. Noble and P. Podvin for providing processing facilities for seismic migration and for advice and guidance. We also thank J.L. Chazelas and all the French National Microtunnel project for making the test site available. Finally, we thank the Colorado School of Mines for making the SU package available to geophysicists as free domain software. We are grateful to Ginette Saracco for proofreading and advice.

REFERENCES

Adler F. 1996. *Tomographie de réflexion à partir des images migrées avant addition*. PhD thesis, University of Pau et des Pays de l'Adour, France.

Bano M. 1996. Constant dielectric losses of ground-penetrating radar waves. *International Geophysical Journal* **124**, 279–288.

Bitri A. and Grandjean G. 1998. Frequency-wavenumber modelling and migration of 2D GPR data in moderately heterogeneous dispersive media. *Geophysical Prospecting* **46**, 287–301.

Bleistein N. 1987. On the imaging of reflectors in the earth. *Geophysics* **52**, 7931–7942.

Botelho M.A., Mufti I.R. and Neto V.P. 1998. Multishot prestack depth migration: an application on real wide-angle reflection and refraction GPR data. 68th SEG meeting, New Orleans, Louisiana, USA, Expanded Abstracts, 1393–1396.

Chazelas J.L. 1996. *Création d'un Site Test pour les Méthodes Géophysiques Appliquées aux Travaux sans Tranchée*. Rapport technique No. 12, Projet National Microtunnels, FSTT.

Claerbout J.F. 1970. Coarse grid calculations of waves in inhomogeneous media with application to delineation of complicated seismic structure. *Geophysics* **35**, 407–418.

Claerbout J.F. 1971. Toward a unified theory of reflector mapping. *Geophysics* **36**, 467–481.

Claerbout J.F. 1972. Downward continuation of moveout-corrected seismograms. *Geophysics* **37**, 741–768.

Cohen J.K. and Stockwell J.W., Jr. 1997. *CWP/SU: Seismic Unix Release 3: A free package for seismic research and processing*. Center for Wave Phenomena, Colorado School of Mines, USA.

Fisher E., McMechan G.A. and Annan A.P. 1992a. Acquisition and processing of wide-aperture ground-penetrating radar data. *Geophysics* **57**, 495–504.

Fisher E., McMechan G.A., Annan A.P. and Cosway S.W. 1992b. Examples of reverse-time migration of single-channel, ground-penetrating radar profiles. *Geophysics* **57**, 577–586.

Gazdag J. 1978. Wave equation migration with the phase-shift method. *Geophysics* **43**, 1342–1351.

Grandjean G., Gourry J.C. and Bitri A. 2000. Evaluation of GPR techniques for civil-engineering applications: study on a test site. *Journal of Applied Geophysics* **45**, 141–156.

Greaves R.J., Lesmes D.P., Lee J.M. and Toksöz M.N. 1996. Velocity variations and water content estimated from multi-offset, ground-penetrating radar. *Geophysics* **61**, 683–695.

Hagedoorn J.G. 1954. A process of seismic reflection interpretation. *Geophysical Prospecting* **2**, 85–127.

Hollender F., Tillard S. and Corin L. 1999. Multifold borehole radar acquisition and processing. *Geophysical Prospecting* **47**, 1077–1090.

Jaya M.S., Botelho M.A., Hubral P. and Liebhardt G. 1999. Remigration of ground-penetrating radar data. *Journal of Applied Geophysics* **41**, 19–30.

Leparoux D. 1997. *Mise au point de méthodes radar pour l'auscultation structurale et texturale de milieux géologiques très hétérogènes (Modélisation, Migration, Expérimentation)*. PhD thesis, University of Rennes 1 and Laboratoire Central des Ponts et Chaussées, France.

Liner C.L. and Liner J.L. 1995. Ground-penetrating radar: a near-face experience from Washington County, Arkansas. *Leading Edge* **14**, 17–21.

Miller D., Oristaglio M. and Beylkin G. 1987. A new slant on seismic imaging: migration and integral geometry. *Geophysics* **52**, 943–964.

Noble M.S., Marsset B., Missiaen T. and Versteeg W. 1996. Near surface 2D and 3D data processing: beyond stack. 58th EAGE conference, Amsterdam, The Netherlands, Extended Abstracts, MO33.

Patterson A.J., Tealby J.M. and Allinson N.M. 1995. GPR imaging with focused migration. 57th EAGE Conference, Glasgow, Scotland, Extended Abstracts, PO53.

Podvin P. and Lecomte I. 1991. Finite difference computation of traveltimes in very contrasted velocity models: a massively parallel approach and its associated tools. *International Geophysical Journal* **105**, 271–284.

Schneider W.A. 1978. Integral formulation for migration in two and three dimensions. *Geophysics* **43**, 49–76.

Stolt R.H. 1978. Migration by Fourier transform. *Geophysics* **43**, 23–48.

Stolte C., Ristow D. and Nick K.P. 1994. Eccentricity-migration for the imaging of pipes in radar reflection data. 56th EAEG meeting, Vienna, Austria, Extended Abstracts, IO14.

Turner G. 1994. Subsurface radar propagation deconvolution. *Geophysics* **59**, 215–223.

Young R.A., Deng Z. and Sun J. 1995. Interactive processing of GPR data. *Leading Edge* **14**, 275–280.